View metadata, citation and similar papers at core.ac.uk

brought to you by CORE

provided by UNT Digital Library

UCRL-JRNL-222558

LAWRENCE
LIVERMORE
NATIONAL
LABORATORY

Direct Observations of Sigma Phase Formation in Duplex Stainless Steels using In Situ Synchrotron X-Ray Diffraction

J. W. Elmer, T. A. Palmer, E. D. Specht

July 3, 2006

Metallurgical Transactions A

Disclaimer

This document was prepared as an account of work sponsored by an agency of the United States Government. Neither the United States Government nor the University of California nor any of their employees, makes any warranty, express or implied, or assumes any legal liability or responsibility for the accuracy, completeness, or usefulness of any information, apparatus, product, or process disclosed, or represents that its use would not infringe privately owned rights. Reference herein to any specific commercial product, process, or service by trade name, trademark, manufacturer, or otherwise, does not necessarily constitute or imply its endorsement, recommendation, or favoring by the United States Government or the University of California. The views and opinions of authors expressed herein do not necessarily state or reflect those of the United States Government or the University of California, and shall not be used for advertising or product endorsement purposes.

Rev : July 24, 2006

Direct Observations of Sigma Phase Formation in Duplex Stainless Steels using In Situ Synchrotron X-Ray Diffraction

J.W. Elmer, T.A. Palmer and E.D. Specht*

Lawrence Livermore National Laboratory, Livermore, CA
*Oak Ridge National Laboratory, Oak Ridge, TN

Abstract

The formation and growth of sigma (σ) phase in 2205 duplex stainless steel was observed and measured in real time using synchrotron radiation during 10 hr isothermal heat treatments at temperatures between 700ºC and 850ºC. Sigma formed in near-equilibrium quantities during the isothermal holds, starting from a microstructure which contained a balanced mixture of metastable ferrite and austenite. In situ synchrotron diffraction continuously monitored the transformation, and these results were compared to those predicted by thermodynamic calculations. Differences between the calculated and measured amounts of sigma, ferrite and austenite suggest that the thermodynamic calculations underpredict the sigma dissolution temperature by approximately 50ºC. The data were further analyzed using a modified Johnson-Mehl-Avrami (JMA) approach to determine kinetic parameters for sigma formation over this temperature range. The initial JMA exponent, n, at low fractions of sigma was found to be approximately 7.0, however, towards the end of the transformation, n decreased to values of approximately 0.75. The change in the JMA exponent was attributed to a change in the transformation mechanism from discontinuous precipitation with increasing nucleation rate, to growth of the existing sigma phase after nucleation site saturation occurred. Because of this change in mechanism, it was not possible to determine reliable values for the activation energy and pre-exponential terms for the JMA equation. While cooling back to room temperature, the partial transformation of austenite resulted in a substantial increase in the ferrite content, but sigma retained its high temperature value to room temperature.

Introduction

Duplex stainless steels (DSS) are often processed to have a balanced microstructure containing approximately 50% austenite and 50% ferrite, which provides them with a desirable combination of hardness, toughness, and corrosion resistance [1]. However, when exposed to temperatures between approximately 600ºC and 1000ºC for sustained periods of time, several undesirable intermetallic phases can form [2, 3]. The σ phase, which has a complex tetragonal crystal structure with a large unit cell, is the most prominent of the intermetallic phases. Sigma is enriched in Cr and Mo relative to the nominal composition of the alloy, and because of this it grows from the ferrite phase which is also enriched in these elements [1, 4].

Once formed, sigma is known to adversely affect the mechanical properties [4-8] and corrosion resistance [9, 10] of DSS alloys. For example, the impact toughness of 2205 DSS has been found to decrease by nearly an order of magnitude when exposed to an extended 850ºC isothermal heat treatment [6]. Decreases in the pitting and crevice corrosion resistance are also pronounced in the presence of σ phase. This decrease in corrosion resistance is attributed to the depletion of Cr and Mo in regions surrounding the newly formed sigma precipitates [10]. As a result, the DSS becomes susceptible to localized corrosion via a mechanism similar to sensitization in austenitic stainless steels.

During elevated temperature processing of DSS and austenitic stainless steel alloys, sigma nucleates heterogeneously and grows from either austenite/ferrite or at ferrite/ferrite grain boundaries present in the microstructure. The amount of ferrite that forms depends on both the alloy composition and the amount of ferrite in the starting microstructure. Thus, larger amounts of σ phase form in DSS alloys than in austenitic stainless steel alloys due to their higher ferrite contents [11-14]. Sigma phase has been observed in cast alloys [15, 16], in weld metal fusion and heat affected zones [17-19], and in continuously cooled [20] duplex stainless steels, indicating its propensity to form under numerous materials processing conditions.

In this investigation, an in situ x-ray diffraction technique using high intensity synchrotron radiation is used to directly observe the transformation of ferrite to sigma phase and secondary austenite in 2205 DSS. These types of in-situ studies have a number of inherent advantages over more conventional optical metallographic techniques in the study of phase transformations. Most importantly, the transformation can be monitored in real time to provide a continuous measurement of the transformations as they occur. Unlike conventional metallographic meas-

urements, the synchrotron technique allows direct observations of complex phase transformations that occur during elevated temperature processing of materials. The results from these experiments directly measured the kinetics of σ phase formation and provided a basis for more in-depth investigations of transformations in DSS alloys at elevated temperatures.

Experimental

Materials

Chemical analysis performed on the 2205 DSS used in this study shows that it contains 22.43%Cr, 4.88%Ni, 3.13%Mo, 0.14% Mn, 0.67%Si, 0.18%N and 0.023%C by weight. This is the same material used during previous investigations that used synchrotron radiation to observe phase transformations during welding [21, 22]. The as-received material, which was taken from 10.8 cm diameter forged bar stock, had been solution mill annealed at 1065ºC for 2.5 hours followed by water quenching to produce a microstructure containing nearly equal amounts of ferrite and austenite. The samples were machined from the bar in an orientation parallel to the extrusion axis. The samples measured 100 mm long by 4.75mm wide by 2 mm thick, and all surfaces were milled to a 62 micron rms finish in preparation for the x-ray diffraction experiments.

Figure 1(a) shows the microstructure of the as-received material, with the austenite being the lightly etched phase (tan/white in color) and the ferrite being the more darkly etched phase (blue/purple in color). The DSS microstructures were revealed using an electrolytic KOH etch (50 gm KOH, 100 mL water) held at a voltage of 5V for approximately 10 s [15]. This etch is used specifically to expose the σ phase present in the microstructure after the isothermal heat treatments, but it also adequately distinguishes the ferrite and austenite phases in both the as received and the heat treated conditions. Quantitative metallographic measurements performed on this alloy in the as-received condition show a ferrite-to-austenite ratio of 54:46 [21]. Figure 1(b) shows microstructure after heat treating at 850ºC for 10 hours. Here sigma is present in volume fractions near 20%, and is the most darkly etched phase (brown/orange/black) in the microstructure. The ferrite continues to etch a blue/purple color and the austenite continues to etch a tan/white color in this figure.

An equilibrium phase diagram for this DSS alloy was calculated using ThermoCalc® version q and the TC Fe2 database including Fe, Cr, Ni, Mo, Mn, Si, C, and N in the model. Figure 2 shows the resulting phase fraction versus temperature plot where equilibrium was calculated by

considering the presence of ferrite, austenite, sigma, nitrides/carbides, and the liquid phases. The calculations indicate that ferrite transforms to a combination of austenite and sigma during heating up to 700 ºC, where ferrite dissapears. Between 700ºC and 800ºC the ferrite does not exist, and sigma partially transforms to austenite as the temperature increases. At 800ºC, ferrite reappears, and sigma continues to decrease until it completely disappears at a temperature of approximately 860ºC. Since the 2205 DSS base metal microstructure is metastable, due to its quenching from 1065ºC, the real microstructure starts off with a significantly different ferrite/austenite ratio than that predicted from the thermodynamic calculations. Because of this, the starting microstructure of the 2205 DSS will approach equilibrium during the isothermal hold differently than if the initial sample had been prepared via a slow cooling process that was closer to equilibrium.

In-Situ X-Ray Diffraction Experiments and Data

In-situ x-ray diffraction experiments were performed using the UNICAT beam line BM-33-C at the Advanced Photon Source (APS) at the Argonne National Laboratory. The focused x-ray beam measured 1.0 mm wide by 0.25 mm high at the sample location and had an energy of 30 keV. During the experiment, the beam impinged on the top surface of the sample at a 5° angle of incidence while the sample was heated at a rate of 20ºC/sec to the desired temperature using a direct resistance heating method. At this angle of incidence, the beam penetrates approximately 7 μm below the surface of the sample given the 160 μm absorption length of these x-rays in iron. A schematic diagram of the experimental setup is shown in Figure 3a, and one of the complete diffraction patterns is shown in Fig 3b. All of the experiments were performed with the sample inside of an environmental chamber and held in a vacuum of approximately 10^{-4} Torr. The X-rays entered and exited the aluminum chamber through Kapton windows.

The diffracted beams were collected using a CCD detector manufactured by Roper Scientific (A99k401, RS/Photometrics) placed 330 mm behind the sample. This detector uses a 6.1 x 6.1 cm^2 array of 1024x1024 pixels spaced 60 microns apart to capture the diffraction patterns. The detector captures the x-ray data by integrating the diffracted beams over a 1 s exposure. Another 2 s are required to clear the data from the CCD detector and transfer it to the computer. For the long duration of these runs, some of the data were acquired at 10 s intervals after the sample reached the isothermal hold temperature in order to reduce the amount of data that was stored.

After the data were recorded, the Debye arcs were converted, using Fit-2D software, into a conventional diffraction plot of intensity versus d spacing. This software integrates the diffracted beam intensity for each arc over the entire two dimensional areal array, yielding the data that can be used to create the diffraction patterns used in the following analyses. Additional details about the data acquisition technique are presented elsewhere [23, 24].

The calculated austenite, ferrite and sigma phase peaks present in each diffraction pattern are summarized in Table 1. This table includes their individual relative peak intensities (I), their d-spacing, 2θ angle, multiplicity factor (M) and structure factor (F^2) as calculated by JPOWD [25] for the 30 keV beam. The ferrite (bcc, a_o=2.881Å) and austenite (fcc, a_o=3.430Å) calculations were performed using the lattice parameters for pure Fe. Although the lattice parameters of ferrite and austenite in pure Fe and those of the DSS alloy are different due to compositional effects, the calculated values for pure Fe can be used to provide a good initial estimate of where the actual ferrite and austenite diffraction peaks will appear for the DSS alloy. Calculations of the diffraction peaks for the sigma phase (tetragonal, a=8.885, c =4.603) were performed using lattice parameters approximately 1% larger than that of the reported FeCr sigma phase [26], which gave the best fit to the actual sigma phase diffraction pattern at room temperature. The results show that three austenite peaks, three ferrite peaks, and a multitude of sigma phase peaks should appear in the diffraction window, which covers about 10 deg of 2θ for the experimental conditions used in this study. Note that the sigma phase peaks reported in Table 1 are only those with a calculated intensity greater than 3%, additional lower intensity peaks are present but were considered to be too low of intensity to be accurately quantified.

Figure 4 shows a room temperature diffraction pattern (upper diffraction pattern), plotted as intensity versus 2θ. This diffraction pattern was taken after the 850ºC heat treatment where a significant amount of sigma had formed, and is compared to the calculated sigma phase peaks (lower diffraction pattern). The indexing of the sigma phase corresponds to the Miller indices of the peaks as summarized in Table 1. It is clear that all of the non-fcc or non-bcc peaks, which appear in the experimental diffraction pattern can be attributed to sigma. Note that the sigma (330), peak 3, overlaps with the fcc (111), and that the sigma (202), peak 4, overlaps with the bcc(110) peaks. Considering the thermodynamic predictions at 850ºC as shown in Fig. 2, ferrite, austenite and sigma should all be present in the equilibrium microstructure, and each of these phases is indeed observed in this diffraction pattern.

Once all the x-ray diffraction data were acquired, the peak areas were measured for each phase and used as a means to estimate their relative amounts in the microstructure as a function of isothermal hold time. To do this, the raw integrated areas from each of the diffraction peaks present in each diffraction pattern were first measured and summed. The peaks used in this measurement were all of the major bcc and fcc peaks in the diffraction window, as indicated in Table 1, plus the eight highest d-spacing peaks of the sigma phase as indicated in Table 1 by the sigma identifications 1-8.

Since some of the diffracted peaks were not accounted for in the analysis due to their low intensity or because they fell outside the 2-θ range of the x-ray detector, the fraction of the diffracted beam for each phase that was captured needs to be corrected to account for this difference. To do this, the calculated integrated intensity for all possible diffraction peaks for each phase was determined and used to represent 100% of the total diffracted intensity for each phase. This calculation takes into account the structure factors for the bcc, fcc, and tetragonal crystal structures of the ferrite, austenite, and sigma phases, respectively, the multiplicity for each peak, and the Lorentz polarization factors as summarized in Table 1 [25]. Next, the integrated intensity of just the diffracted peaks used in the analysis of the synchrotron data was determined in the same way, and compared to the total diffracted intensity for each phase. Doing this, it was determined that 69.1% of the bcc diffraction, 60.4% of the fcc diffraction and 58.1% of the sigma phase diffraction was accounted for in the diffraction peaks examined from the synchrotron experiments. The measured diffraction intensity of each phase was corrected using these factors, and then the fraction of each phase was determined by taking the ratio of the corrected diffraction intensity of each phase to the sum of the diffraction intensities for all three phases. This calculation was done on every diffraction pattern throughout the isothermal hold, allowing the volume fraction of each phase to be determined as a function of isothermal hold time.

Results and Discussion

Direct Observations of Phase Transformations During Isothermal Heat Treating

Table 2 summarizes the results of the isothermal heat treatments, showing the different temperatures, holding times and amounts of each phase at the beginning and end of the isothermal hold. One of the runs (750ºC) was terminated 7 hours into the isothermal hold due to an equipment malfunction, however all the other samples were held for the complete 10 hrs. In this table,

the volume fractions of each phase at the beginning and end of each heat treatment, and the time at which sigma is first observed are shown. These data are compared with the equilibrium values as predicted by Thermocalc, and this comparison will be discussed in more detail later.

The results of the in situ x-ray diffraction experiments consist of a series of diffraction patterns, which for the extended runs here can number in the thousands. One useful way to display this data is in the form of a pseudo-color plot where the diffraction patterns are lined up with time along the y-axis, d-spacing along the x-axis, and the intensities of the diffraction peaks represented by different colors. Figure 5 shows one of these plots, for the initial 2000 seconds of the run at 800ºC. The heating initiates at t=0s, and immediately all of the fcc and bcc diffraction peaks shift to higher d-spacings due to the thermal expansion effect while the sample is being heated. The sample reaches 800ºC at t=48s, and during the isothermal hold the intensity of the bcc peak immediately began to decrease while the intensity of the fcc peaks increased. At t=96s, a low intensity sigma (410) peak first appears. With increased holding time, the intensity of this peak increases and additional sigma peaks appear. In this figure, only six of the eight sigma peaks are observed, since two of the sigma peaks overlap with fcc and bcc peaks. Initially, the sigma (202) is hidden below the bcc (110) and the sigma (330) is hidden below the fcc (111). With time, the bcc phase decreases to nearly 0 percent at this temperature, and the hidden sigma (202) peak remains. Small differences in the d-spacing between the sigma (202) and the bcc (110) allow them to be distinguished as the amount of bcc decreases, however, the sigma (330) never appears since the fcc (111) remains at high intensity throughout the entire experiment.

The changes in the diffraction peak intensity can be correlated with changes that are taking place in the volume fractions of each of the three phases during the isothermal hold. Using the run at 800ºC as an example, Figure 6 plots the measured volume fractions of these phases as a function of isothermal heat treatment time for the first hour of the hold where the majority of the transformation takes place. The alloy begins with a ferrite/austenite ratio of approximately 1:1, which decreases considerably as ferrite partially transforms to austenite and sigma. The sigma phase, which first appears at t=96s, rapidly increases to approximately 90% of its equilibrium value within the first 1 hr of the run. Similar transformations were observed at the other temperatures. However, the rates of transformation and the amounts of sigma produced varied with temperature.

Figure 7 compares the results of all of the synchrotron data, showing the fractions fcc, bcc, and sigma as a function of isothermal hold time at each of the four temperatures. The bcc ferrite phase is shown in Fig 7(a), indicating that it continually decreases throughout each of the isothermal holds and reaching zero or near-zero values at 750ºC and 800ºC. However, at 700ºC, the transformation kinetics appears to slow for the ferrite to reach its equilibrium value, since several percent ferrite remains at the end of the 10 hr run. At 850ºC, approximately 3% bcc phase remains at the end of the 10 hr run, which may be near its equilibrium value, since Thermocalc predicts some residual bcc phase at this temperature (see Fig. 2). The fcc phase is shown in Fig 7b, where it continually increases to values between 75 and 80% during the isothermal holds. The trends suggest that the fcc phase is reaching near equilibrium values at all of the temperatures. The amount of sigma phase is shown in Fig. 7c, where each temperature appears to produce a different final volume fraction of sigma. The amount of sigma ranges from 19.8% to 22.7%, as summarized in Table 2, with the lowest amount of sigma being found at the highest temperature (850ºC). As with the other phases, near equilibrium volume fractions appear to be reached at all of the temperatures except 700ºC.

During the early stages of the transformation, sigma forms preferentially at ferrite/austenite interphase boundaries and ferrite/ferrite grain boundaries, and grows into the ferrite phase via a transformation mechanism involving diffusion. Since both nucleation and diffusional growth of sigma are thermally activated processes, temperature will have a significant effect on the kinetics of the transformation. In order to look at this more closely, Fig. 8 compares the measured volume fraction of sigma that forms during the early stages of the transformation at each of the four temperatures. The times where sigma was first observed are further summarized in Table 2, indicating that the minimum time observed to form sigma was 96 s, at a temperature of 800ºC. Slightly longer times of 153 s and 192 s were observed at 850ºC and 750ºC respectively, and a much longer time of 2003 s was observed at the lowest temperature of 700ºC. The amount of sigma present when it was first detected was approximately 1% in all four cases.

The data were further plotted in Fig. 9 to show the time temperature relationships for the formation of sigma at seven different amounts of transformation, between 1% to 99% sigma. In this plot, the measured maximum amount of sigma that formed at each temperature was used to represent 100% of the possible amount of sigma that could form (see Table 2), and this value decreased with increasing temperature. The shape of the curves indicates that the early stages of

sigma phase nucleation and growth are occurring by C-curve kinetics with the nose at approximately 800ºC.

The measured amounts of sigma for the three temperatures where near equilibrium amounts of sigma formed (750ºC, 800ºC and 850ºC) exceed those predicted by Thermocalc (see Fig. 2). At 750ºC and 800ºC, the difference is only a few percent. At 850ºC, however, the difference is nearly a factor of 6. Since the amount of sigma decreases to zero at temperatures above its solvus, a reduction in the amount of sigma is expected at higher temperatures. However, the temperature at which the rapid decrease in sigma occurs appears to be underpredicted by Thermocalc. Whereas Thermocalc predicts zero percent sigma at 860ºC, the synchrotron measurements show approximately 15% sigma at this temperature. Comparing the calculated values with the measured values shows that the two sets of data would be very similar if the Thermocalc data were shifted approximately 50ºC higher, i.e., the Thermocalc predictions at 800ºC seem to match the measured values at 850ºC etc. Additional synchrotron measurements are planned in the future to more closely investigate temperatures above 850ºC in order to determine the dissolution temperature more exactly for this alloy.

Isothermal Kinetics of Sigma Phase Formation

TTT diagrams have been produced for a cast version of the 2205 alloy (CD3MN) having a similar composition to the DSS 2205 used in this investigation, and another cast DSS alloy, CD3MWCuN which has a higher Cr and Mo content that promotes sigma formation [16]. These investigations on cast materials utilized conventional metallographic techniques to measure the sigma content after the isothermal holds, and the results show different kinetics for sigma formation even though they are both duplex stainless steels. These TTT diagrams indicate a wide variation in the times required to nucleate and to completely transform the alloy to sigma, and show the nose of the TTT curves to be between 800ºC and 850ºC. For example, the minimum time to form 1% sigma at the nose of their respective TTT curves is 10 min for the CD3MN alloy and 5 min for the CD3MWCuN from tabulated data in this paper [16]. The minimum time required to form 99% sigma at the nose of the respective TTT curves is 7000 min for the CD3MN alloy versus 70 min for the CD3MWCuN alloy. The faster transformation kinetics of the CD3MWCuN alloy were attributed to its higher Cr and Mo content.

Comparing the kinetics of sigma formation in the 2205 DSS with the cast versions discussed above, the 2205 DSS appears to have a slightly lower nose temperature and takes about twice as long as the CD3MWCuN alloy to complete its transformation. The DSS 2205 appeared to transform more quickly at first than the cast alloys, having the shortest amount of time to reach 1% sigma. However, the apparent faster kinetics of the DSS 2205 may be the result of the higher accuracy and continuous measurement of sigma made possible by the synchrotron technique, as compared to the metallographic method used in the other investigation where 1% transformation may be difficult to observe and quantify since only a few data points were taken at short times. The minimum time for complete transformation of the 2205 DSS in this investigation, defined by 99% or more of the possible sigma phase formed, was found to take approximately twice as long as the CD3MWCuN alloy, but occurred much faster than in the CD3MN alloy.

Phase transformation kinetic analysis of the synchrotron data on the 2205 DSS was performed using a Johnson Mehl Avrami (JMA) method to describe the overall transformation rate. This approach is often represented by the following expression [27]:

$$f_e(t) = 1 - \exp\{-(kt)^n\} \qquad \text{(eq. 1)}$$

where $f_e(t)$ is the extent of the transformation as a function of time t measured relative to the equilibrium value of the product phase, n is the JMA exponent, and k is a rate constant given as:

$$\mathrm{k} = \mathrm{k}_0 \exp(-\frac{\mathrm{Q}}{\mathrm{RT}}) \qquad \text{(eq. 2)}$$

In this expression, k_0 is a pre-exponential constant, Q is the activation energy of the transformation including the driving forces for both nucleation and growth, R is the gas constant and T is the absolute temperature (K). The JMA exponent, n, is often correlated to different types of nucleation and growth conditions, and is an indicator of the kinetics responsible for the transformation [28]. One way to determine the value of the JMA exponent from experimental data is to linearize eq. (1) by plotting the $\ln(\ln(1-f_e(t)))$ versus ln(t), where n can be determined from the slope of the data on these coordinates.

Figure 10 plots the fraction sigma formed for each of the four temperatures on the JMA coordinates. In this plot, it is clear that the data do not follow a linear trend with ln(t), and that all of the curves start off with a steep slope that decreases as the transformation continues. The initial slope, between 1% and 5% sigma, for each of the four sets of data is summarized in Table 4. These slopes give the JMA exponent, n, to be approximately 7.0. However, n continuously

decreases, and towards the end of the transformation n approaches a value of approximately 0.75 at the three highest temperatures where the transformation went to completion. This change in slope indicates a change in the JMA exponent, and suggests that the mechanism for the transformation is changing as the transformation proceeds. Because of this, reliable values of the activation energy, Q, and the JMA pre-exponential term, ko, were not able to be determined for this transformation, however, the changing slope and its values are useful nevertheless.

Although the JMA exponent can't be used to precisely identify the mechanism, it can be used as an indicator of the type of nucleation and growth conditions that are occurring. According to Christian [28], a JMA exponent above 4, like those observed at low fractions of sigma, would indicate that the transformation is taking place by either a discontinuous precipitation or an interface controlled growth mechanism, with a nucleation rate that increases with increasing fraction transformed. Evidence for this is indicated in Fig. 11, which shows the microstructure after a 30 min hold at 800°C and is in the early nucleation and growth stages for this alloy. It is clear that sigma preferentially forms at ferrite/austenite and ferrite/ferrite boundaries. At longer hold times, the particles take on more of a blocky or elongated appearance (see Fig 1b). If the transformation initially begins with a nucleation rate that is increasing, the nucleation rate would be expected to decrease as the preferred nucleation sites become more saturated as the transformation continues.

Sigma is known to nucleate and grow from ferrite (α) with the simultaneous formation of secondary austenite (γ_2) by the transformation $\alpha \rightarrow \gamma_2 + \sigma$ [29]. Although the transformation mechanism doesn't appear to be characterized perfectly well in the literature, it is likely that one of the major modes for decomposition of ferrite occurs by a discontinuous precipitation mechanism. This mechanism is also referred to as cellular precipitation, and is similar to a eutectoid transformation in steels [29], and would fit with a JMA exponent greater than 4.

In the case of 2205 DSS, the secondary austenite and sigma phases would grow through the cooperative partitioning of elements between them [29, 30]. Microstructural evidence suggests that the secondary austenite first forms at the ferrite/austenite boundaries, causing Cr and Mo to be rejected into the ferrite ahead of the secondary austenite phase. When the concentration of the ferrite is enriched sufficiently in Cr and Mo, sigma nucleates and grows, sometimes alongside the secondary austenite and other times as isolated sigma particles that become surrounded by the secondary austenite. The time required for Cr and Mo to enrich accounts for the

delay in nucleation of sigma phase which is most evident at 700ºC (see Fig. 8). Figure 12 shows a high magnification micrograph of the partially transformed microstructure from the 700ºC isothermal hold, and indicates the major microstructural constituents. The original austenite (γ) is outlined by a series of small precipitates (C/N) that are believed to be nitrides/carbides that formed at the original ferrite/austenite interface [15]. Secondary austenite and σ grow cooperatively into the original ferrite. The discontinuous precipitation of sigma appears most clearly at the top of the original austenite grain, where multiple cells of austenite are growing with sigma forming in the cusps between them. Isolated sigma phase precipitates also appear in the ferrite, where they most likely nucleated heterogeneously from preexisting inclusions or defects in the ferrite phase and are accompanied by secondary austenite.

At longer transformation times, the JMA exponent decreases to values of approximately 0.75, which can indicate thickening of large plates or growth of particles after nucleation site saturation was achieved [28]. This transformation mechanism would occur when the majority of available nucleation sites are already taken and the transformation continues by growth of the existing sigma phase particles. Thus, the formation of sigma in this alloy is one that appears to be strongly influenced by the nucleation conditions since growth of the sigma is slow at these temperatures. Even at the highest temperatures and longest isothermal hold times (see Fig 1b), the sigma particles retain their individual shapes, and never appear to grow larger than about 10μm in size.

According to Grong [31], the activation energy for heterogeneous nucleation, Q_d, can be estimated from isothermal transformation data by plotting it on 1/T versus ln(t) coordinates for a given amount of transformation. A C-curve plotted on these coordinates retains its C shape, but is distorted and has well defined asymptopes, and Q_d can be determined from the product of the slope of the low temperature asymptope and the universal gas constant, R. At low temperatures, below the nose of the C-curve, Q_d represents the activation energy for atomic transport across the nucleating phase interface, and can be used as a relative indicator of the ease of nucleation. To determine Q_d, Fig. 14 plots the synchrotron data for 1, 10, 25, 50 and 75% sigma formation relative to their equilibrium values on the 1/T versus ln(t) coordinates. Q_d was then determined from the data taken between the two lowest temperatures, 700ºC and 750ºC, and the results are summarized in Table 5. The results indicate that Q_d tends to increase with fraction transformed, and has values that vary from 357kJ/mole to 482 kJ/mole. These activation energies can be com-

pared to the values for diffusion of sigma forming elements, Cr and Mo, in the ferrite and austenite phases. Diffusion of Mo and Cr in the austenite and ferrite phases of pure iron vary between values of 230 and 290 kJ/mole depending on the diffusing specie and its concentration [32]. Therefore, Q_d is significantly higher than the activation energy for diffusion in this system. The higher activation energy indicates that nucleation is likely a controlling factor in the formation of sigma, and indicates that long range diffusion to the growing sigma may not be limiting its formation.

Austenite to Ferrite Transformation During Cooling to Room Temperature

During the isothermal hold, the amount of ferrite decreased as it transformed to a mixture of sigma and secondary austenite. The maximum amount of ferrite at the end of the hold was shown to vary with temperature, from only 3.2% for the sample held at 700ºC to nearly 0% for the sample held at 800ºC. However, after the samples were cooled back to room temperature, the microstructure revealed significantly higher amounts of ferrite present in each. Fig 1b showed the post heat treated microstructure of the sample held at 850ºC, clearly indicating the presence of large amounts of ferrite, which are on the order of 30%. The ferrite that appears in this sample at the end of the experiment was created by the back transformation of austenite to ferrite as the sample cooled to room temperature. This partial transformation of austenite to ferrite is expected based on the thermodynamic calculations shown in Fig 2, which indicate that austenite begins to transform to ferrite at temperatures below about 700ºC.

The amount of ferrite that formed in one of the samples (800ºC) was monitored during cooling to follow the phase transformations back to room temperature. Figure 13 shows the results of this measurement and compares the ferrite, austenite and sigma phase contents from the start to the end of the run. This plot shows that the austenite in the starting material (49.6%) increased to 79.8% during the isothermal hold, but then decreased to 45.1% during cooling to room temperature. Thus the final amount of austenite in this sample is only slightly less than the initial amount. The ferrite on the other hand had an initial value of 50.4% which rapidly decreased to near zero values during the isothermal hold. During cooling, the ferrite reappeared and increased to 34.7% as the austenite transformed to ferrite. While the austenite and ferrite were transforming during cooling, sigma did not transform at all, retaining 20.2% sigma at room temperature. In the end there was a net decrease in the ferrite content of the sample of 15.7% and a net de-

crease in the austenite of 4.5%, which was compensated for by the retained sigma at room temperature of 20.2% in this sample.

The final ferrite/austenite ratio of the sample held at 800ºC was measured to be approximately 0.8 (34.7/45.1) at room temperature, which is significantly below that of the starting material of approximately 1.1 (50.4/49.6). This low ferrite/austenite ratio after the 800ºC hold is the result of an incomplete transformation of austenite to ferrite, and is significantly lower than that predicted from equilibrium thermodynamics due to kinetic limitations during the rapid cooling of the sample back to room temperature. Thus, the direct observation of the phases existing at elevated temperature made possible with in-situ x-ray diffraction, provided confirming evidence of the phases and conditions that are not present in post experimental observations, nor can be accurately predicted by thermodynamic calculations alone.

Summary and Conclusions

The ability to directly observe phase transformations using synchrotron radiation provides an ideal means to study complex phase transformations with unambiguous observations of the phases that are present. Using this technique, the formation of sigma and the corresponding ferrite and austenite transformations were able to be studied with higher accuracies than can be provided by conventional techniques, and from the results the following conclusions were made.

1. The formation and growth of sigma in 2205 DSS was observed and measured in real time using synchrotron radiation during isothermal heat treating at temperatures between 700ºC and 850ºC, and for times up to 10 hr.
2. Ferrite was observed to transform to a mixture of sigma and austenite phases during the 10 hr hold times. The measured amounts of sigma were compared to those predicted by Thermocalc version q using the TCFe2 database. Differences between the calculated and measured amounts of sigma exist, suggesting that the thermodynamic calculations underpredict the maximum temperature where sigma can exist by about 50ºC (860ºC calculated versus over 900ºC estimated from the measurements).
3. The in-situ synchrotron data were quantified to measure the transformation rates and final volume fractions of each of the phases at the different temperatures. The results show that hold times of 3 hours were long enough to create near equilibrium transformations at all tem-

peratures except at 700ºC, which required more than 10 hours for the transformations to go to completion.

4. A TTT diagram was created for the sigma transformation in this 2205 DSS, showing that the nose of the curve is at approximately 800ºC, which is similar to the results from other investigators who find the nose at temperatures between 800ºC and 850ºC.
5. A JMA analysis of sigma transformation kinetics revealed that the transformation rates were significantly different at low and high amounts of sigma. At low sigma fractions, the initial JMA exponent, n, was found to be approximately 7.0. However, n was shown to continuously decrease to values of approximately 0.75 near the end of the transformation. Reliable values of the activation energy, Q, and the JMA pre-exponential term, ko, were not able to be determined for this transformation due to this variation in n.
6. The change in the JMA exponent was attributed to changes in the transformation mechanism whereby the higher values during the early stages of transformation corresponded to discontinuous precipitation mechanism with increasing nucleation rate, the higher values during the later stages of the transformation corresponded to growth of the existing sigma after nucleation site saturation occurred.
7. The back transformation of austenite to ferrite during cooling after the isothermal hold was measured, showing that the austenite decreases back to near its original value after the sample has cooled and the ferrite increases to a value significantly less than its original value, indicating that sigma formed primarily from the ferrite phase.

Acknowledgements

The LLNL portion of this work was performed under the auspices of the U. S. Department of Energy by UC, Lawrence Livermore National Lab., under Contract No. W-7405-ENG-48. The ORNL portion of this work was sponsored by the U.S. Department of Energy Division of Materials Sciences and Engineering under contract No. DE-AC05-00OR22725 with UT-Battelle, LLC. The UNICAT facility at the Advanced Photon Source (APS) is supported by the U.S. DOE under Award No. DEFG02-91ER45439, through the Frederick Seitz Materials Research Laboratory at the University of Illinois at Urbana-Champaign, the Oak Ridge National Laboratory (U.S. DOE contract DE-AC05-00OR22725 with UT-Battelle LLC), the National Institute of Standards and Technology (U.S. Department of Commerce) and UOP LLC. The APS is supported by the U.S. DOE, Basic Energy Sciences, Office of Science under contract No. W-31-109-ENG-38. The authors would like to thank Professor T. DebRoy of the Pennsylvania State University for reviewing this article and adding helpful suggestions, and would also like to thank Mr. Jackson Go of LLNL for performing the optical metallography.

References

1. H.D. Solomon and T.M. Devine, "Duplex Stainless Steels – A Tale of Two Phases", in *Duplex Stainless Steels*, ed. by R.D. Lula, (American Society for Metals, Metals Park, OH, pp. 693-756, 1983.

2. L. Karlsson, "Intermetallic Phase Precipitation in Duplex Stainless Steels and Weld Metals: Metallurgy, Influence on Properties, Welding and Testing Aspects", *WRC Bulletin*, 438 1999.

3. J.-O. Nilsson, "Super Duplex Stainless Steels", *Mater. Sci. Technol*., Vol. 8, pp. 685-700, 1992.

4. E. O. Hall and S. H. Algie, "The Sigma Phase," *Metallurgical Reviews*, Review No. 104, The Institute of Metals, Vol. 11, pp. 61-88, 1966,

5. J.-O. Nilsson, P. Kangas, T. Karlsson, and A. Wilson, "Mechanical Properties, Microstructural Stability and Kinetics of σ-Phase Formation in 29Cr-6Ni-2Mo-0.38N Superduplex Stainless Steel", *Metall.Mater. Trans A*, Vol. 31A, pp. 35-45, 2000.

6. Y.S. Ahn and J.P. Kang, "Effect of Aging Treatments on Microstructure and Impact Properties of Tungsten Substituted 2205 Duplex Stainless Steel", *Mater. Sci. Technol*., Vol. 16, pp. 382-388, 2000.

7. J. Li, T. Wu, and Y. Riquier, "σ Phase Precipitation and its Effect on the Mechanical Properties of a Super Duplex Stainless Steel", *Mater. Sci. Engin*., Vol. A174, pp. 149-156, 1994.

8. T.H. Chen, K.L. Weng, and J.R. Yang, "The Effect of High-Temperature Exposure on the Microstructural Stability and Toughness Property in a 2205 Duplex Stainless Steel", *Mater. Sci. Engin. A*, Vol A338, pp. 259-270, 2002.

9. J.-O. Nilsson and A. Wilson, "Influence of Isothermal Phase Transformations on Toughness and Pitting Corrosion of Super Duplex Stainless Steel SAF 2507", *Mater. Sci. Technol*., 9, pp. 545-554, 1993.

10. Y.S. Ahn, M. Kim, and B.H. Jeong, "Effect of Aging Treatments and Microstructural Evolution on Corrosion Resistance of Tungsten Substituted 2205 Duplex Stainless Steel", *Mater. Sci. Technol*., Vol. 18, pp. 383-388, 2002.

11. J. Barcik, "The Kinetics of σ-Phase Precipitation in AISI 310 and AISI 316 Steels", *Metall. Trans. A*, Vol. 14A, 635-641, 1983.

12. J. Barcik, "Mechanism of σ-Phase Precipitation in Cr-Ni Austenitic Steels", *Mater. Sci. Technol*., Vol. 4, pp. 5-15, 1988.

13. J. Barcik, "The Process of σ-Phase Solution in 25 Pct Cr-20 Pct Ni Austenitic Steels", *Metall. Trans. A*, 18A, pp. 1171-1177, 1987.

14. A.V. Kington and F.W. Noble, "Formation of σ Phase in Wrought 310 Stainless Steel", *Mater. Sci. Technol*., Vol. 11, , pp. 268-275, 1995.

15. E. Johnson, Y-J. Kim, L.S. Chumbley, and B. Gleeson, "Initial Phase Transformation Diagram Determination for the CD3MN Cast Duplex Stainless Steel", *Scripta Mater*., 50, pp. 1351-1354, 2004.

16. Y-J. Kim, L.S. Chumbley, and B. Gleeson, "Determination of Isothermal Transformation Diagrams for Sigma-Phase Formation in Cast Duplex Stainless Steels CD3MN and CD3MWCuN", *Metall. Mater. Trans. A*, 35A, pp. 3377-3386, 2004.

17. J.-O. Nilsson, T. Huhtala, P. Jonsson, L. Karlsson, and A. Wilson, "Structural Stability of Super Duplex Stainless Steel Weld Metals and Its Dependence on Tungsten and Copper", *Metall. Mater. Trans. A*, 27A, pp. 2196-2208, 1996.

18. J.M. Vitek and S.A. David, "The Aging Behavior of Homogenized Type 308 and 308CRE Stainless Steel", *Metall. Trans. A*, 18A, pp.1195-1201, 1987.

19. T. H. Chen and J. R. Yang, "Microstructural Characterization of Simulated Heat Affected Zone in a Nitrogen-Containing 2205 Duplex Stainless Steel," Mat. Sci. Eng. A, Vol. 338, pp. 166-181, 2002.

20. T. H. Chen and J. R. Yang, "Effects of Solution Treatment and Continuous Cooling of σ-Phase Precipitation in a 2205 Duplex Stainless Steel," *Materials Science and Engineering A*, Vol. 311, pp. 28-41, 2001.

21. T. A. Palmer, J. W. Elmer, S. S. Babu, "Observations of Ferrite/Austenite Transformations in the Heat Affected Zone of 2205 Duplex Stainless Steel Spot Welds Using Time Resolved X-Ray Diffraction." *Materials Science and Engineering A*, Vol. 374, pp. 307-321, 2004.

22. T. A. Palmer, J. W. Elmer, and Joe Wong, "In-Situ Observations of Ferrite/Austenite Transformations in Duplex Stainless Steel Weldments Using Synchrotron Radiation," *Science and Technology of Welding and Joining*, Vol. 7(3), pp 159-171, 2002.

23. J.W. Elmer, T.A. Palmer, S.S. Babu, and E.D. Specht, "In-Situ Observations of Lattice Expansion and Transformation Rates of α and β Phases in Ti-6Al-4V", *Materials Science and Engineering A*, 391(1-2), 104-13, 2004.

24. J.W. Elmer, T.A. Palmer, S.S. Babu, and E.D. Specht, "Low Temperature Relaxation of Residual Stress in Ti-6Al-4V," *Scripta Mater*., 52(10), 1051-6, 2005.

25. JPOWD: *Materials Data Inc*., Livermore, Build 11/17/2005.

26. H. L. Yakel, "Atom distribution in sigma-phases. I. Fe and Cr distribution in a binary phase equilibrated at 1063, 1013 and 923 K", *Acta Crystallographica B*, Vol. 39, pp 20-28, 1983.

27. J. W. Elmer, T. A. Palmer, W. Zhang, and T. DebRoy, "Advanced Techniques for In-Situ Monitoring of Phase Transformations During Welding Using Synchrotron-Based X-Ray Diffraction," accepted for publication in the 7th *International Conference on Trends in Welding Research, ASM International*, Pine Mountain Georgia, May, 2005.

28. J. W. Christian: *The Theory of Transformations in Metals and Alloys, 2nd Edition, Part I*, Oxford: Pergamon, 1975.

29. B. Josefsson, J.-O. Nilsson and A. Wilson, " Phase Transformations in Duplex Stainless Steels and the Relation Between Continuous Cooling and Isothermal Heat Treatment," in *Duplex Stainless Steel '91*, edited by J. Charles and S. Bernhardsson, Les Editions de Physique, France, Vol 1, pp 67-78, 1991.

30. C-S. Huang and C-C. Shih, "Effects of Nitrogen and High Temperature aging on Sigma Phase Precipitation of Duplex Stainless Steel," *Materials Science and Engineering A*, Vol. 402, 66-75, 2005.

31. O. Grong: *Metallurgical Modeling of Welding*, The Institute of Materials, 1994.

32. C. J. Smithells, E. A. Brandes, G. B. Brook: *Smithells Metal Reference Book*, 7th Edition, Butterworth-Heinemann Ltd., Oxford, United Kingdom, 1992.

Table 1. Summary of calculated diffraction peaks at 30 keV. Unit cell volumes are given in the first column. The peak ID column refers to the indexing of the sigma phase in Fig 4, starting with the lowest 2θ peak observed in the detector window, sigma (002). Sigma phase peaks with less than 3% intensity are not listed nor indicated in Fig 4.

Phase	Peak ID	hkl	2θ (deg.)	d (Å)	Intensity (%)	Structure Factor (F^2)	M
Austenite		111	11.98	1.980	94.3	4944	8
(fcc)		200	13.84	1.715	59.7	4178	6
40.35 ($Å^3$)		220	19.62	1.213	69.4	2427	12
Ferrite		110	11.64	2.037	100	1273	12
(bcc)		200	16.50	1.440	32.0	816	6
23.91 ($Å^3$)		211	20.24	1.176	90.2	574	24
Sigma		311	9.89	2.398	4.45	1664	16
(tetragonal)	1	002	10.30	2.302	18.16	54350	2
363.4 ($Å^3$)	2	410	11.01	2.155	73.15	54737	8
	3	330	11.33	2.094	33.47	50086	4
	4	202	11.61	2.044	30.53	22843	8
	5	212	11.91	1.992	61.6	23043	16
	6	411	12.16	1.952	100	37411	16
	7	331	12.45	1.906	50.1	37489	8
	8	222	12.78	1.857	11.65	8718	8
	9	312	13.33	1.780	13.74	5142	16
	10	322	14.11	1.682	3.75	1403	16
	11	431	14.32	1.658	3.95	1476	16
	12	511	14.57	1.630	3.52	1316	16
	13	432	16.90	1.407	3.13	1170	16
	14	512	17.11	1.389	3.02	1128	16
	15	522	17.73	1.341	6.73	2518	16
	16	532	18.72	1.271	21.45	8025	16
	17	550	18.93	1.257	7.86	11768	4
	18	413	19.03	1.250	27.43	10264	16
	19	602	19.10	1.245	11.07	8283	8
	20	333	19.22	1.238	13.98	10457	8
	21	612	19.29	1.233	9.17	3432	16
	22	702	19.50	1.220	18.82	14083	8
	23	551	19.63	1.212	10.67	7983	8
	24	622	19.85	1.199	5.66	2117	16
	25	542	20.28	1.188	4.94	1849	16
	26	721	20.18	1.180	12.9	4830	16
	27	004	20.69	1.151	11.3	128	2

Table 2. Summary of volume fractions measured at the beginning of the heating cycle and at the end of the isothermal holds. The equilibrium values, as determined by Thermocalc, are shown for comparison.

Amount of Phase	Isothermal hold temperature			
	700ºC	750ºC	800ºC	850ºC
Start of hold				
Ferrite (%)	57.2	55.0	50.4	53.5
Austenite (%)	42.8	45.0	49.6	46.5
Time, first sigma (s)	2003	192	96	157
End of hold				
Time (s)	36070	25007	35951	36241
Ferrite (%)	3.2	0.29	.05	1.9
Austenite (%)	78.3	77.2	79.8	78.3
Sigma (%)	18.5*	22.7	20.2	19.8
Thermocalc				
Ferrite (%)	0	0	0	31.6
Austenite (%)	78.6	80.6	82.5	65.0
Sigma (%)	21.4	19.4	17.5	3.4

* Transformation not completed at end of 10 hour isothermal hold.

Table 3. Summary of measured times required to form given amounts of σ phase in the micro-structure.

Sigma, % of equilib-rium value	700ºC		750ºC		800ºC		850ºC	
	sigma actual	time	sigma actual	time	sigma actual	time	sigma actual	time
(%)	(%)	(s)	(%)	(s)	(%)	(s)	(%)	(s)
1	0.24	2291	0.23	276	0.20	108	0.20	153
5	1.20	3521	1.14	312	1.01	132	0.99	181
10	2.40	4379	2.27	384	2.02	156	1.98	238
25	6.00	8840	5.68	559	5.05	228	4.95	422
50	12.0	17390	11.4	888	10.1	408	9.90	890
75	18.0	35990	17.0	2184	15.2	1056	14.9	2777
90	21.6	*	20.4	4452	18.2	2748	17.9	6493
95	22.8	*	21.5	6306	19.2	4884	18.9	8707
99	23.8	*	22.5	11205	20.0	8256	19.7	15855

* Transformation <90% complete in 10 hrs, 24% sigma estimated if completely transformed.

Table 4. Results of the JMA calculations for sigma phase formation at each of the four temperatures. Initial and final refer to the early and later stages for the transformation respectively.

Temperature (ºC)	n initial	n final
700	4.7	-
750	7.8	0.75
800	6.7	0.68
850	7.0	0.73

Table 5. Results of the activation energy calculations for the nucleation, Q_d, of sigma phase.

Q_d	1%	10%	25%	50%	75%
(kJ/Mole)	357	395	442	482	466

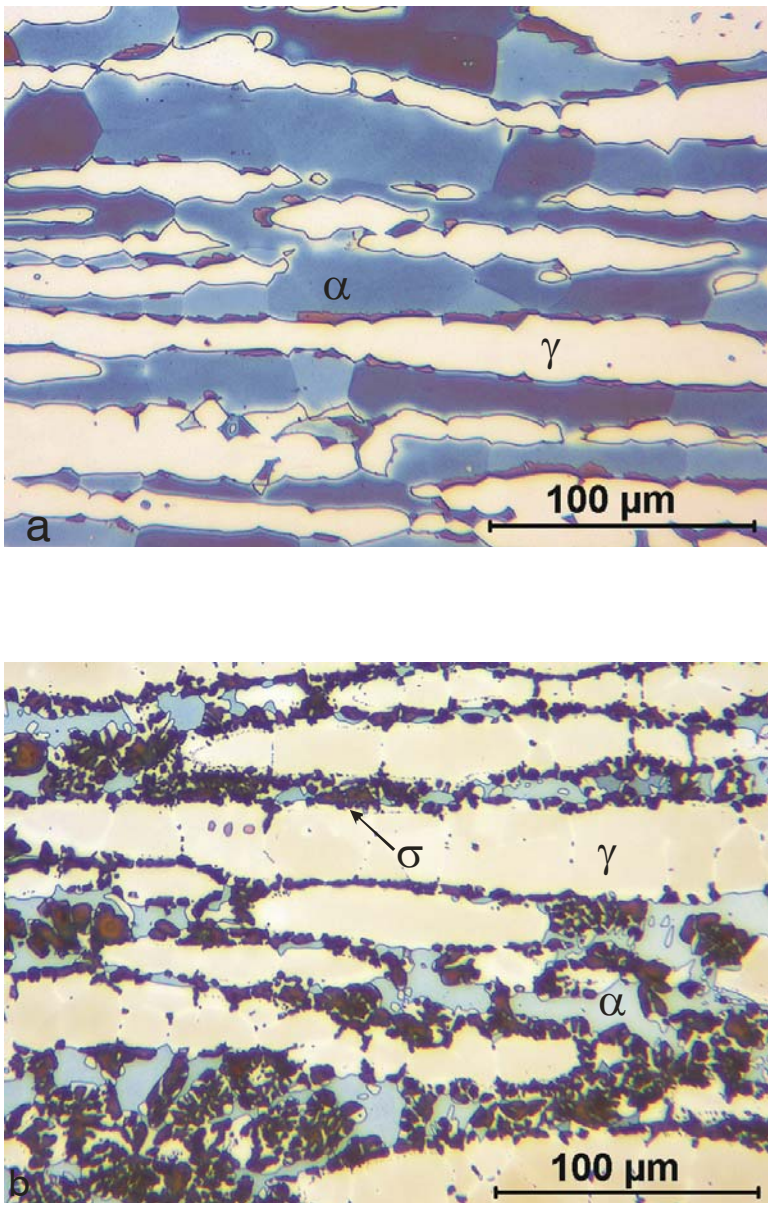

Figure 1: Optical micrographs showing a) ferrite, α, etches blue/purple in color, and austenite, γ, etches tan/white in the base metal microstructure, and b) σ phase, which etches black/brown in color, and appears after the 10 h heat treatment at 850°C.

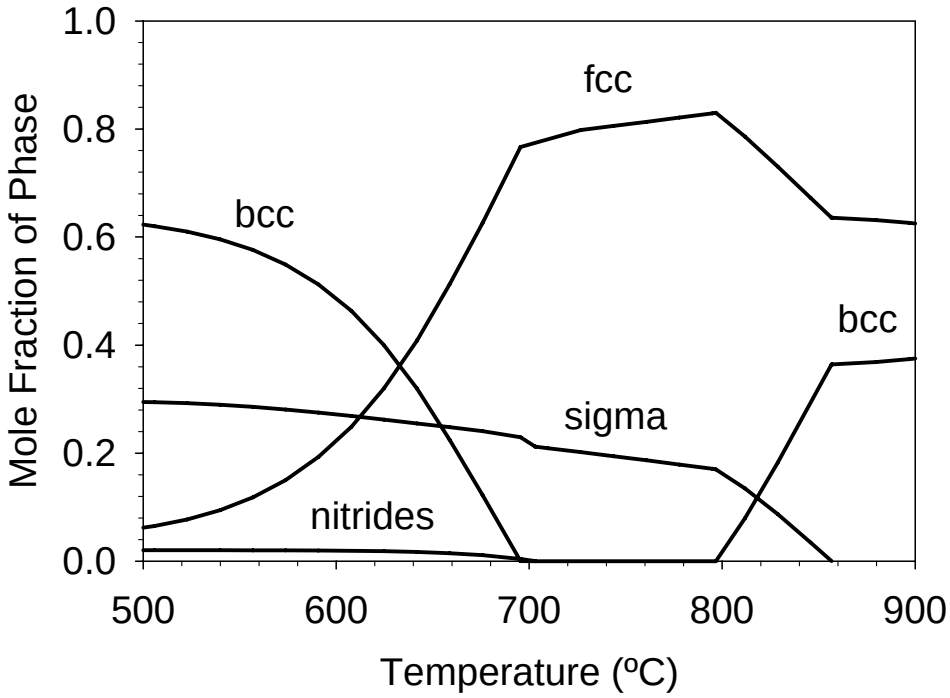

Figure 2: Calculated phase fractions for the 2205 DSS alloy used in this study. The Y-axis in plotted in mole fraction, where one mole is an Avogadro's number of total atoms.

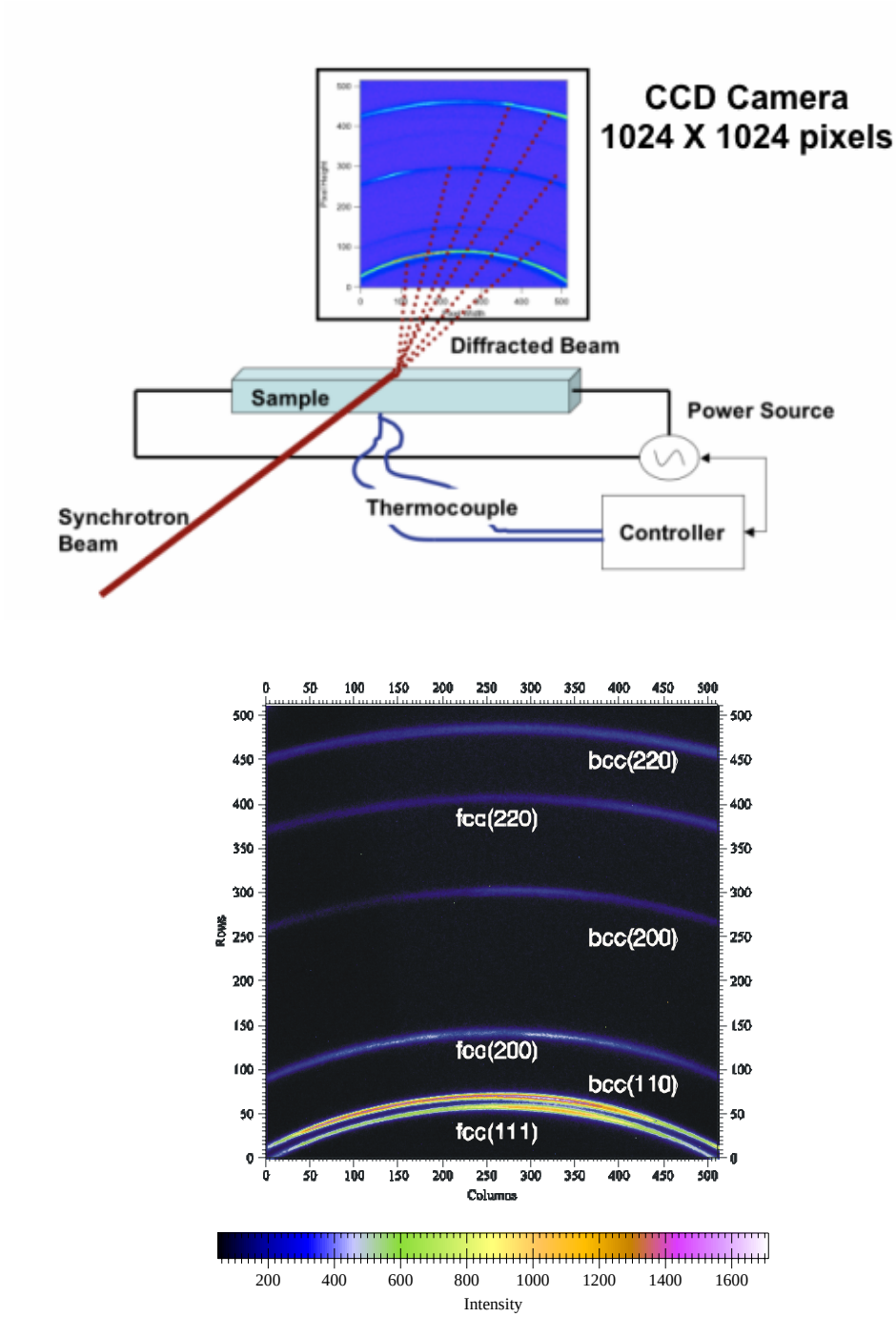

Figure 3: a) Schematic diagram of the x-ray setup used for in situ observations of phase transformations under controlled heating and cooling conditions. b) Plot showing the partial Debye circles obtained using the CCD detector for the 2205 DSS in the as-received condition.

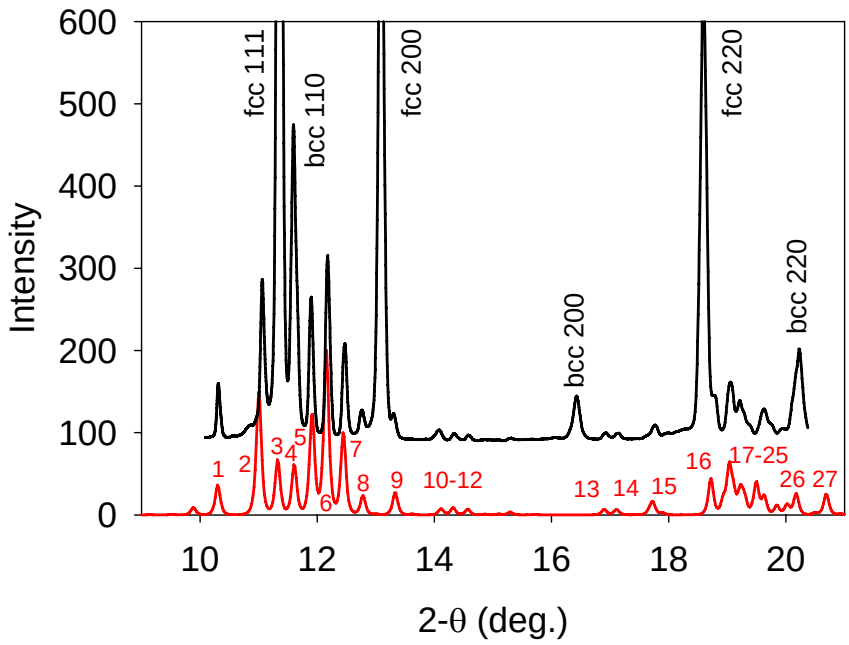

Figure 4: Comparison of the room temperature diffraction pattern after heat treating to form sigma phase (black line) with the calculated diffraction pattern of the sigma phase (red line). Indexing numbers for the sigma phase correspond to the peaks summarized in Table 1. Note that the sigma (330), peak 3, overlaps with the fcc (111), and that the sigma (202), peak 4, overlaps with the bcc (110) peaks.

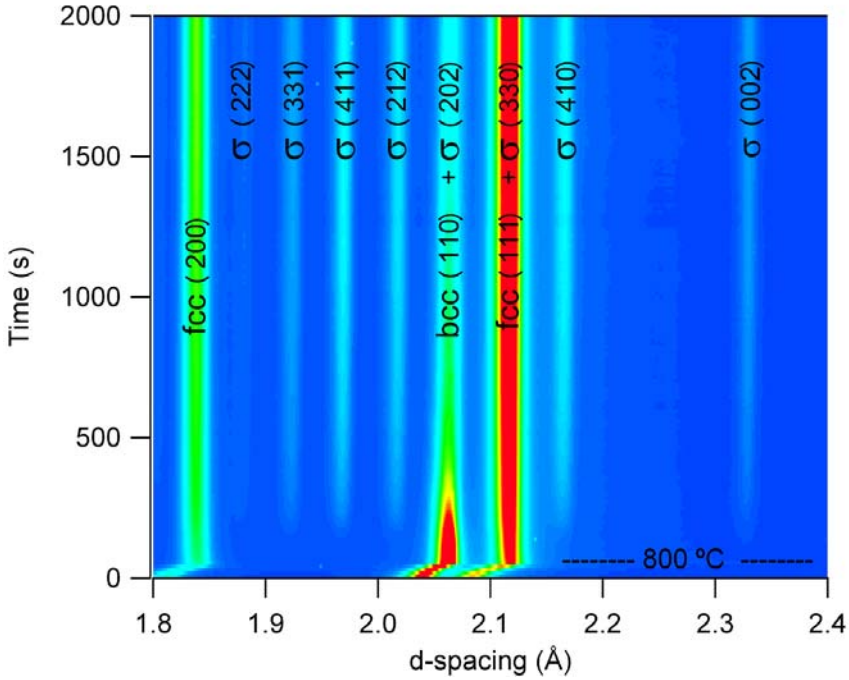

Figure 5: Pseudo-color plot (red corresponds to the highest intensity, blue corresponds to the lowest intensity) of high d-spacing diffraction peak intensities for the first 2000s of the isothermal hold. The heating initiates at t=0s, followed by a rapid increase in d-spacing of the peaks until the isothermal hold temperature of 800ºC is reached.

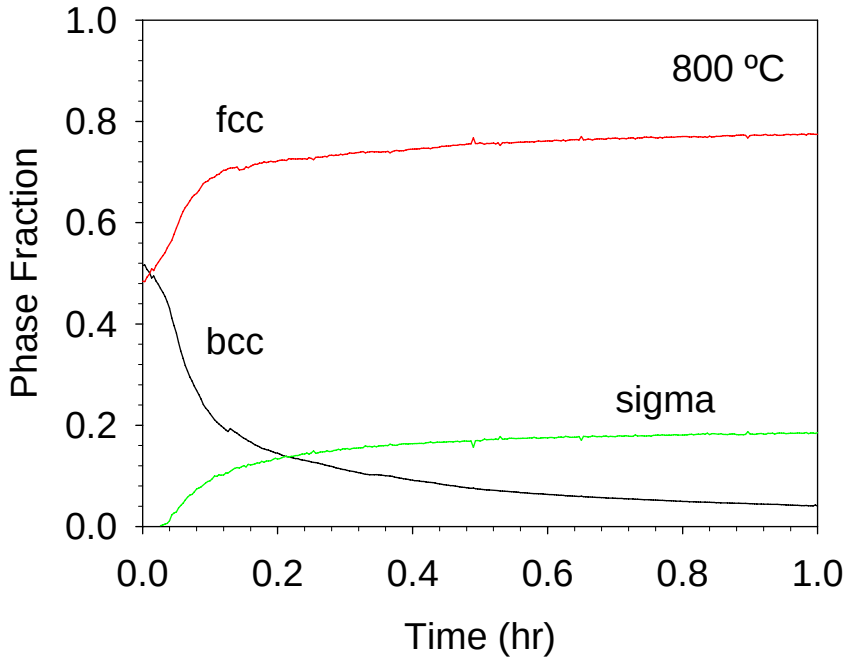

Figure 6: Summary of the measured fractions of the ferrite (bcc), austenite (fcc) and sigma phases as a function of time at 800ºC for times up to 1 hr.

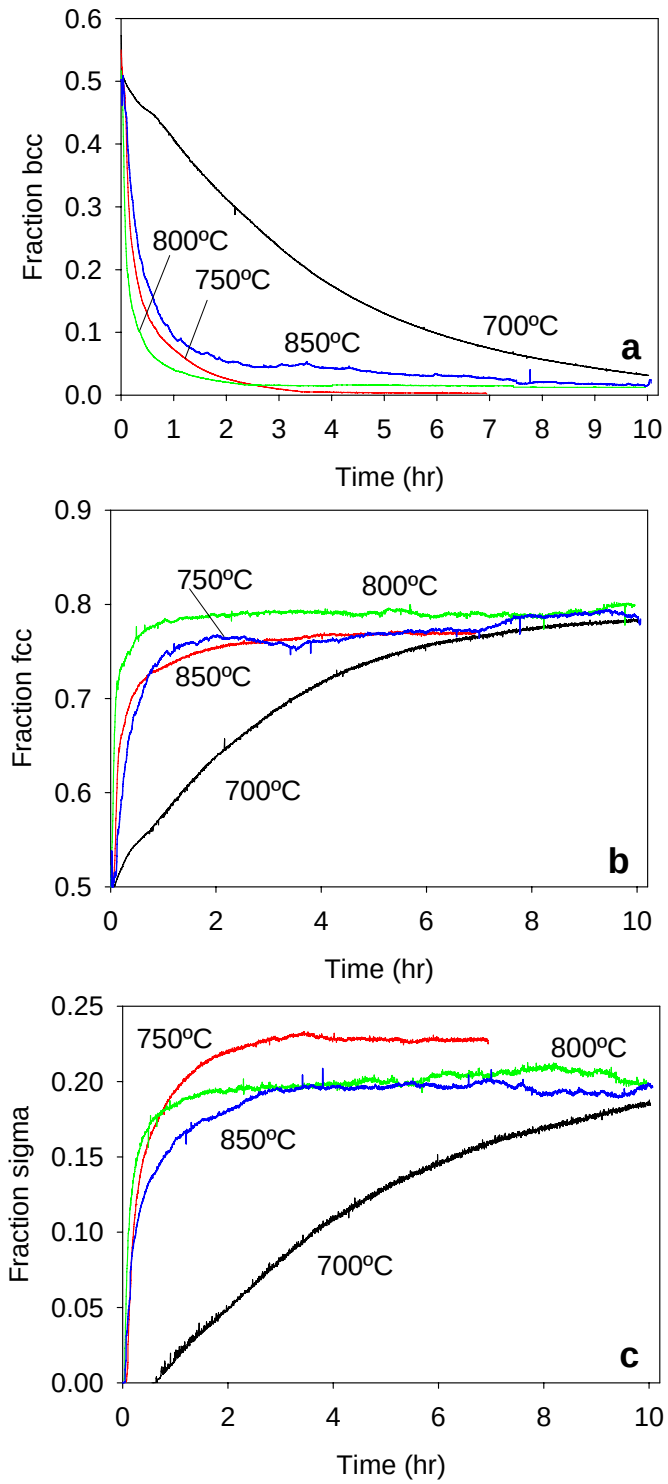

Figure 7: Results from the in-situ synchrotron measurements plotting the fractions of a) ferrite, b) austenite, and c) sigma during the isothermal holds at each of the four temperatures.

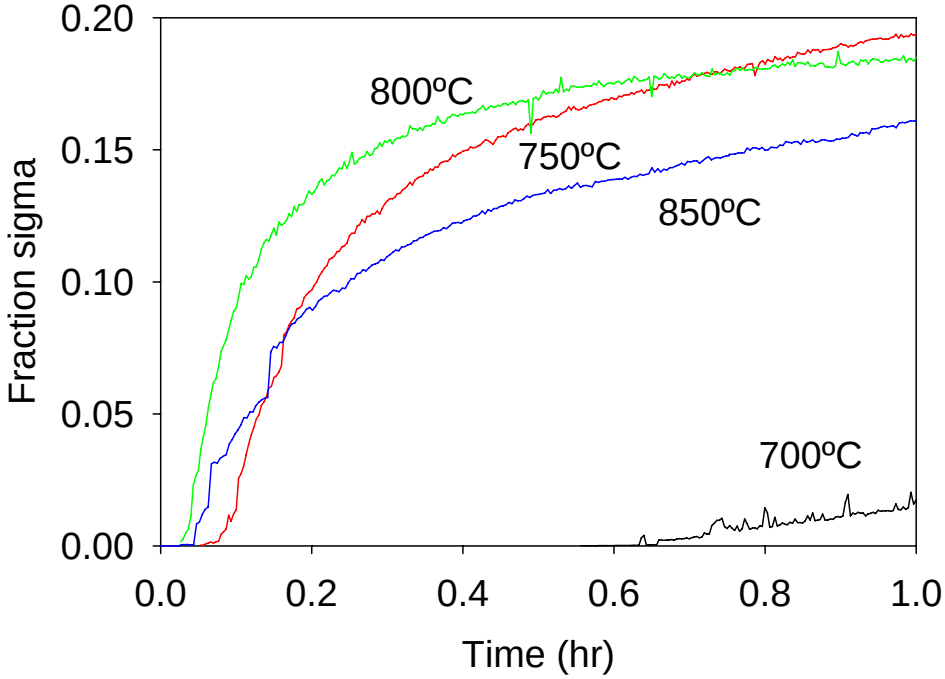

Figure 8: Fraction sigma formed during the first 1 hour of the isothermal holds at each of the 4 temperatures.

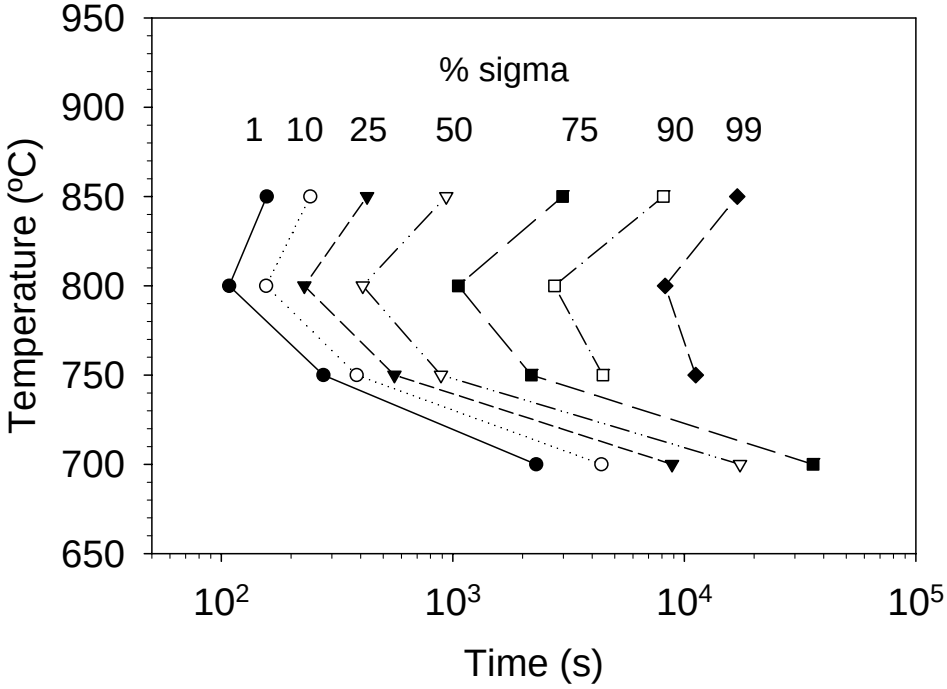

Figure 9: Plot showing the measured amount of sigma, relative to its equilibrium value, plotted versus log of the isothermal hold time at the 4 different temperatures. C-curve kinetics are apparent, with the nose occurring at approximately 800º C.

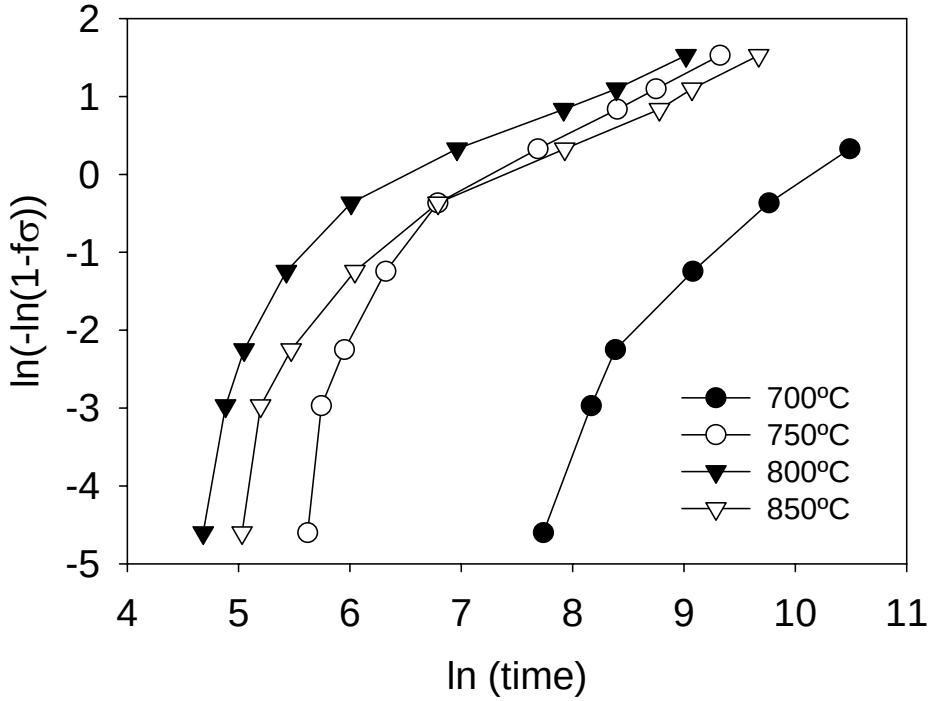

Figure 10: JMA plot of the sigma phase fraction plotted versus ln transformation time (s) at each of the four isothermal temperatures. The non-linearity suggests a change in the transformation mechanism between low and high fractions of sigma phase.

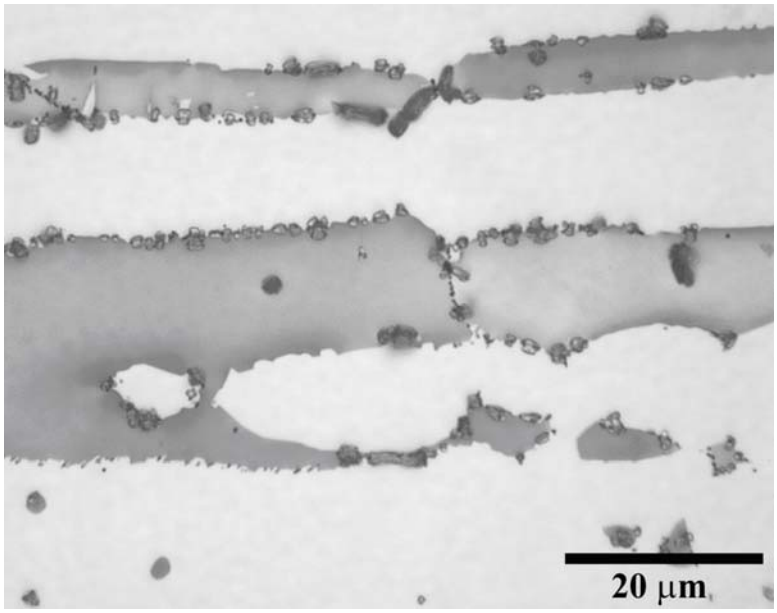

Figure 11: Initial stages of sigma phase formation shown after a 800ºC hold for 30 min. The sigma phase precipitates form preferentially at ferrite/austenite and ferrite/ferrite boundaries.

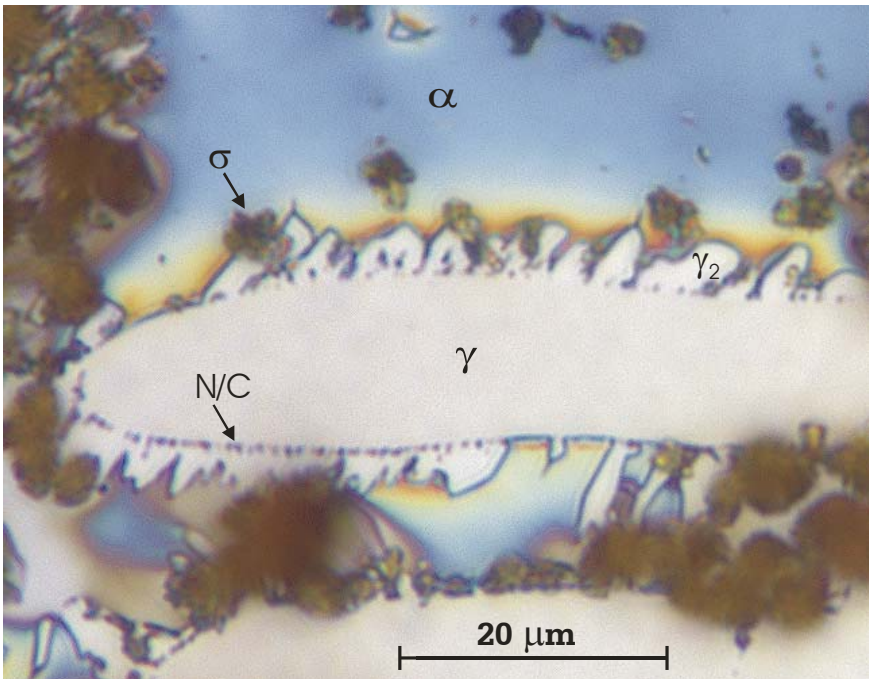

Figure 12: Micrograph taken after the 700ºC hold. The original austenite (γ), ferrite (α), secondary austenite (γ_2), nitrides/carbides at the original austenite/ferrite interface (N/C), and sigma phase (σ) are indicated. The discontinuous precipitation mode of the $\alpha \rightarrow \gamma_2 + \sigma$ transformation can be seen along the top side of the original austenite grain.

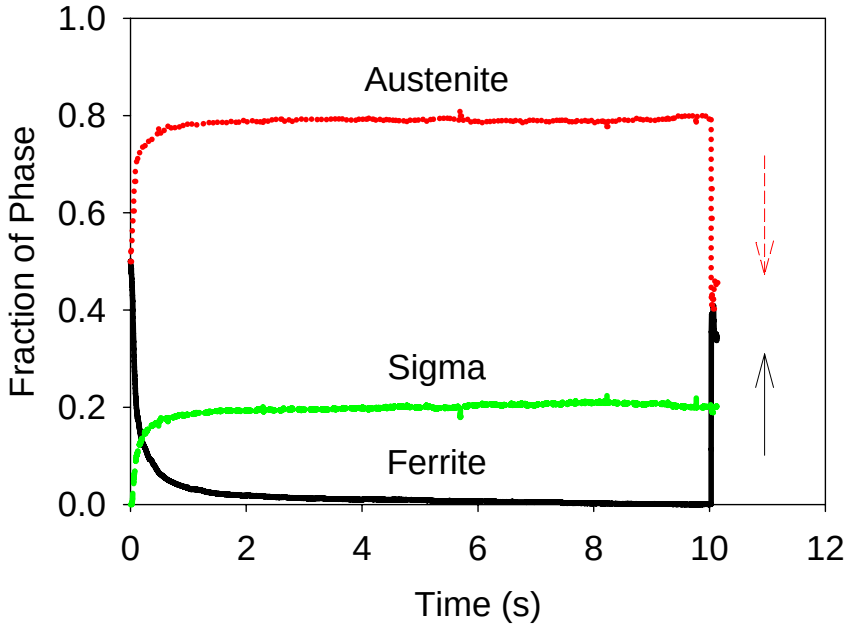

Figure 13: Measured ferrite, austenite and sigma phases for the entire run at 800ºC, showing the partial transformation of austenite (from 79.8% to 45.1%) back to ferrite (from 0.05% to 34.7%) during the final cooling stage of the run. The sigma phase was unaffected during cooling.

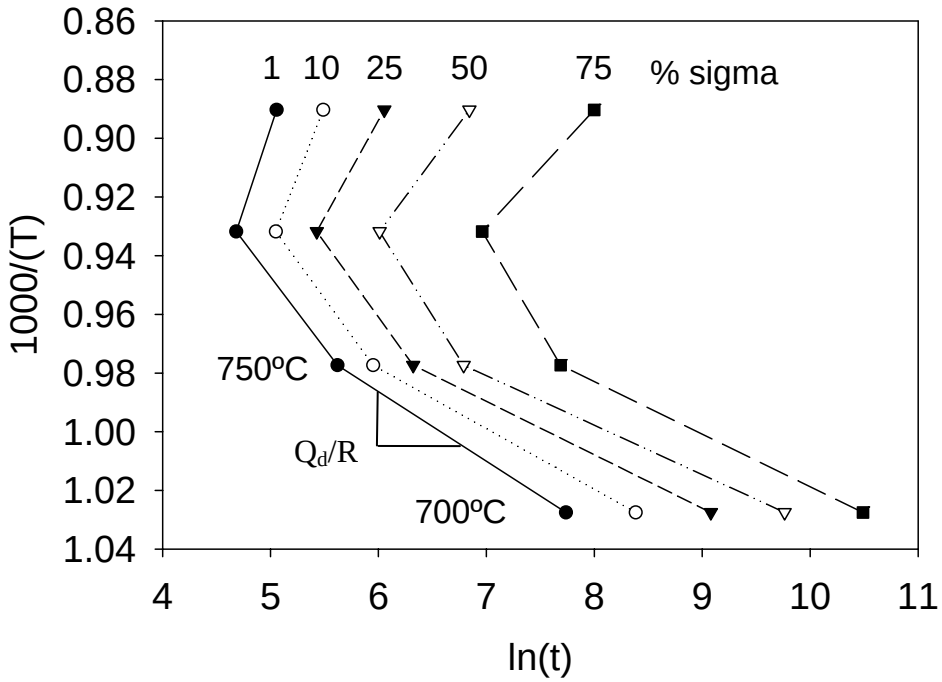

Figure 14: Sigma phase in percent of the equilibrium value, plotted on 1/T versus ln(t) coordinates. The activation energy for nucleation can be estimated from the slope of the curve at the lower temperatures between 700 and 750°C.